Irreversible electroporation for the treatment of localized prostate cancer: a summary of imaging findings and treatment feedback

Matthijs J. Scheltema
Arnoud W. Postema
Daniel M. de Bruin
Mara Buijs
Marc R. Engelbrecht
M. Pilar Laguna
Hessel Wijkstra
Theo M. de Reijke
Jean J.M.C.H. de la Rosette

PURPOSE
Imaging plays a crucial role in ablative therapies for prostate cancer (PCa). Irreversible electroporation (IRE) is a new treatment modality used for focal treatment of PCa. We aimed to demonstrate what imaging modalities can be used by descriptively reporting contrast-enhanced ultrasonography (CEUS), multiparametric magnetic resonance imaging (mpMRI), and grey-scale transrectal ultrasound (TRUS) results. Furthermore, we aimed to correlate quantitatively the ablation zone seen on mpMRI and CEUS with treatment planning to provide therapy feedback.

METHODS
Imaging data was obtained from two prospective multicenter trials on IRE for localized low- to intermediate-risk PCa. The ablation zone volume (AZV) seen on mpMRI and CEUS was 3D reconstructed to correlate with the planned AZV.

RESULTS
Descriptive examples are provided using mpMRI, TRUS, and CEUS for treatment planning and follow-up after IRE. The mean AZV on T2-weighted imaging 4 weeks following IRE was 12.9 cm^3 (standard deviation [SD]=7.0), 5.3 times larger than the planned AZV. Linear regression showed a positive correlation (r=0.76, P = 0.002). For CEUS the mean AZV was 20.7 cm^3 (SD=8.7), 8.5 times larger than the planned AZV with a strong positive correlation (r=0.93, P = 0.001). Prostate volume is reduced over time (mean= -27.5%, SD=11.9%) due to ablation zone fibrosis and deformation, illustrated by 3D reconstruction.

CONCLUSION
The role of imaging in conjunction with IRE is of crucial importance to guide clinicians throughout the treatment protocol. CEUS and mpMRI may provide essential treatment feedback by visualizing the ablation zone dimensions and volume.

From the Departments of Urology (M.J.S. ✉
m.j.scheltema@amc.nl, A.W.P., M.B., M.P.L., T.M.R.,
J.JMCH.D.R.), Biomedical Engineering and Physics
(D.M.B.) and Radiology (M.R.E.), AMC University
Hospital, Amsterdam, The Netherlands; Signal
Processing Systems (H.W.), Eindhoven University of
Technology, The Netherlands.

F ocal therapy is increasingly being used for the treatment of localized or recurrent prostate cancer (PCa) with the intention to treat all significant (i.e., high-volume Gleason 6 or any Gleason 7) PCa lesions while minimizing collateral damage to adjacent vital structures (e.g., neurovascular bundle, urethra, urinary sphincter, and rectal wall). Of all available focal therapy modalities, irreversible electroporation (IRE) is a novel ablative modality based on electroporation (1). Cell death is induced by delivering high-voltage electrical pulses between two or more electrodes (2, 3).

The first phase I-II trials for localized PCa have shown the feasibility and safety of IRE (4–8). Good short-term functional preservation and oncologic control of the ablation zone has been reported (4–6), histopathologic confirmation of the ablation zone showed no residual tumor within the ablation zone in these patients. However, in the pilot study of Murray et al. (7), 4 out of 25 patients had residual tumor on biopsy 6 months following IRE, possibly within the ablation zone. It is challenging to determine whether the biopsy needle is within or adjacent to the ablation zone since grey-scale transrectal ultrasonography (TRUS) is not able to visualize the ablation zone (9) and multiparametric magnetic resonance imaging (mpMRI) at 6 months shows prostate deformations and no clear distinction between treated and untreated tissue (see below). Using the Likert scale (3–5), Valerio et al. (8) reported a suspicion for residual PCa on mpMRI in 6 patients (6/34), but only obtained histopathologic

confirmation in 1 out of 6 patients (Gleason score 3+4).

Consensus statements provide guidance on trial design and the use of imaging for focal therapy. The most recent reports recommend to perform mpMRI both in the planning and follow-up of focal therapy (10, 11). Focal high-intensity focused ultrasound or cryotherapy treatment protocols often include imaging-based follow-up with 6 monthly or annual mpMRI (12). The study endpoints of these protocols are imaging based, without any standardized biopsy endpoint, highlighting the necessity of a profound understanding of mpMRI.

The goal of focal therapy, to treat all significant PCa lesions while minimizing collateral damage to adjacent vital structures, can only be obtained by knowledge of lesion location using image-guidance and imaging feedback on the ablated zone. Besides one phase 1 trial evaluating the ablation zone 4 weeks following IRE treatment with contrast-enhanced ultrasonography (CEUS) and mpMRI (9), no studies have been published on the use of prostate imaging with IRE. No imaging modality has been quantitatively validated in the follow-up following IRE and particularly little is published about the IRE-specific changes seen on imaging during and in the follow-up of IRE. In order to perform focal therapy using IRE, clinicians should have an understanding on which imaging modalities can be used and which imaging results can be expected during different stages of the treatment protocol using IRE. Therefore, we aim to provide an overview on several imaging modalities used in conjunction with IRE by descriptively reporting the utility of CEUS, mpMRI and grey-scale TRUS for treatment planning, procedure guidance and follow-up of IRE. Moreover, at present no imaging modality is able to visualize the extent of the ablation zone during an IRE procedure. In order to provide therapy feedback through imaging, the ablation zone volume (AZV) seen on mpMRI and CEUS was quan-

titatively 3D reconstructed to correlate with the planned AZV.

Methods

The data used for this report were obtained from two prospective multicenter studies and the international IRE registry (clinicaltrials.gov NCT02255890). In the currently ongoing first cohort, 16 patients have received primary IRE because of organ-confined (D'Amico) low- to intermediate-risk PCa. Both CEUS and mpMRI were performed at baseline and used for imaging-based treatment planning for needle placement. Three-dimensional histology lesion localization and grading was obtained with transperineal template-mapping biopsies (TTMB). Grey-scale TRUS was used for procedure guidance, whereas CEUS, mpMRI, and TTMB were performed at 6 months to follow the evolution of the ablation zone and to assess oncologic control. At 1 year, CEUS and mpMRI were performed. The institutional review board (IRB) approved the study protocol (clinicaltrials.gov NTC01835977).

In the second trial (completed) 16 patients were treated with IRE for organ-confined PCa. As part of the ablate and resect design, all patients underwent a radical prostatectomy 4 weeks following IRE. From these patients mpMRI and CEUS data are available at baseline and 1 month follow-up after IRE. This trial was approved by the IRB (clinicaltrials.gov NCT01790451). Inclusion and exclusion criteria and study procedures of both trials have been published elsewhere (13, 14). Written informed consent was obtained from all participants and both clinical trials are conducted in accordance with the Declaration of Helsinki.

Multiparametric MRI

MpMRI was performed using the PI-RADS v2 (15) guidelines on two different MRI scanners (1.5T AVANTO, Siemens and 3.0T Ingenia, Philips). The detailed mpMRI procedures in both trials have been described extensively (9, 14). All mpMRI results were interpreted by a single specialized uroradiologist. If mpMRI and/or CEUS showed a suspicious lesion for PCa in biopsy-naive patients or patients receiving repeat biopsies for active surveillance, fusion targeted biopsies were performed in the work up for the second trial. Lesions were delineated for mpMRI-TRUS fusion with ProFuse (Eigen) software and subsequently targeted using the fusion system (Artemis, Eigen). AZVs were 3D reconstructed with 3D reconstruction software (Amira, FEI) as described previously (9).

Grey-scale transrectal ultrasonography

TRUS was performed in all patients for IRE procedure guidance and during TTMB. An ultrasound system (Preirus Hi Vision, Hitachi) with a biplanar probe (EUP-U533) was used. Prostate dimensions were calculated and both the entire longitudinal and transverse axes were visualized to assure a complete range of motion for needle placement.

Contrast-enhanced ultrasonography

For CEUS imaging an intravascular microbubble ultrasound contrast agent (SonoVue, Bracco) is combined with TRUS using an endocavity probe (Phillips IU22, Philips Healthcare, Bothell, USA). The detailed CEUS procedures are described previously (14). The prostate is visualized in 4 planes from base, mid-base, mid-apex to apex. Before each 2-minute recording a bolus of 2.4 mL ultrasound contrast agent is administered intravenously, followed by a 3-minute pause to allow contrast agent breakdown. These planes are recorded using the fusion device (Artemis, Eigen) and with prostate landmarks for future targeting or follow-up. Additional base-to-apex transversal sweeps and left-to-right lateral sweeps were recorded using CEUS to evaluate the ablation zone post-IRE. AZVs were 3D reconstructed with software (Amira, FEI) as described elsewhere (9). Contrast ultrasound dispersion imaging methods (CUDI) (16) were used for computer-aided quantified analysis and to provide maps of contrast CUDI parameters to identify regions of interest.

Transperineal template-mapping biopsies

TTMB were performed using biplanar TRUS-guidance in combination with template mapping using the same transperineal grid that is used for prostate brachytherapy (Bard). This technique is recommended for patient selection and follow-up after focal therapy (17). If mpMRI and/or CEUS showed lesions suspicious for PCa and fusion targeted biopsies were not obtained previously, additional targeted biopsies were taken using cognitive targeting during TTMB.

IRE procedure

All patients received antibiotic prophylaxis (Ciprofloxacin 500 mg, Bayer) and a transurethral catheter before the IRE procedure. Patients were under general anesthesia and positioned in the lithotomy position, the biplanar TRUS-probe and brachytherapy grid were used for electrode placement. The IRE procedure was performed using the NanoKnife™ IRE System (AngioDynamics). Three to six needle electrodes were used for each ablation, delineating the tumor. The electrode

position, active tip length (1.5–2 cm) and prostate dimensions were entered into the Nanoknife™ console which then calculated and displayed the 2D ablation zone. In total 90 electrical pulses were delivered between each electrode pair with a range of 1.500–3.000 V/cm, to obtain a direct current of 20–40 amp. A deep muscle relaxation agent (Rocuronium, Pfizer) was administered to prevent severe muscle contractions.

In a previous ablate and resect study it has been shown that all tissue within the electrode configuration was ablated (5). Therefore, we consider the area within the electrode configuration as the AZV. Treatment planning AZVs were measured as described previously (5), using image analysis software (ImageJ, FIJI), multiplied by the active tip length to calculate the AZV.

Statistical analysis

The correlation between the 3D reconstructed volumes of CEUS, mpMRI and treatment planning were visualized using a scatterplot (x/y). A linear regression analysis was performed including a Pearson correlation coefficient (r) as measures of correlation. Dependent variables were the volume on MRI/CEUS and the independent variable was the treatment planning volume. The error related to 3D reconstruction was calculated by dividing the AZV by the number of planes for both mpMRI and CEUS. However, for CEUS the errors were too small to display (high number of planes).

Results

As with other focal ablative therapies for PCa, mpMRI is used for patient selection and preoperative treatment planning. The exact demonstration of the location of the PCa lesion(s) is essential for the IRE electrode placement, in particular the relation to the neurovascular bundle, urethra, and bowel (Fig. 1a), as IRE ablation may affect these structures. Needle electrodes need to be placed around the lesion to guarantee effective ablation which has been shown to occur within the zone between electrodes (5, 18). To illustrate, in Fig. 1a the electrodes are placed around the PCa lesion seen on mpMRI (histopathologically confirmed with mpMRI-TRUS fusion targeted biopsies; PCa Gleason 4+3, >50%). In this patient CEUS identified the same lesion (Fig. 1b). TTMB can be used for patient selection and tumor localization in conjunction with mpMRI, if mpMRI is not available or to extensively sample the prostate to diagnose undetected PCa by mpMRI (19, 20). During the TTMB procedure suspicious lesions on mpMRI or CEUS can be targeted using either cognitive or system fusion.
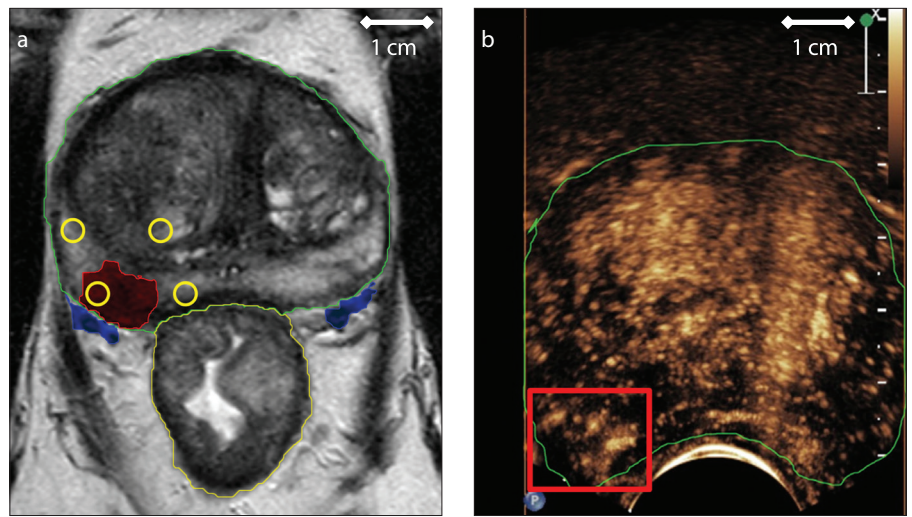

Figure 1. a,b. An anatomical overview **(a)** of the prostate *(delineated in green)* can be seen with the rectum *(delineated in yellow)*, the neurovascular bundles *(blue)* and the prostate cancer (PCa) lesion *(red)*. The *yellow circles* denote the irreversible electroporation (IRE) electrode locations in relation to the tumor. Contrast-enhanced ultrasonography (CEUS) image **(b)** of the same PCa lesion shows increased rapid focal contrast-uptake marked with a *red square*.
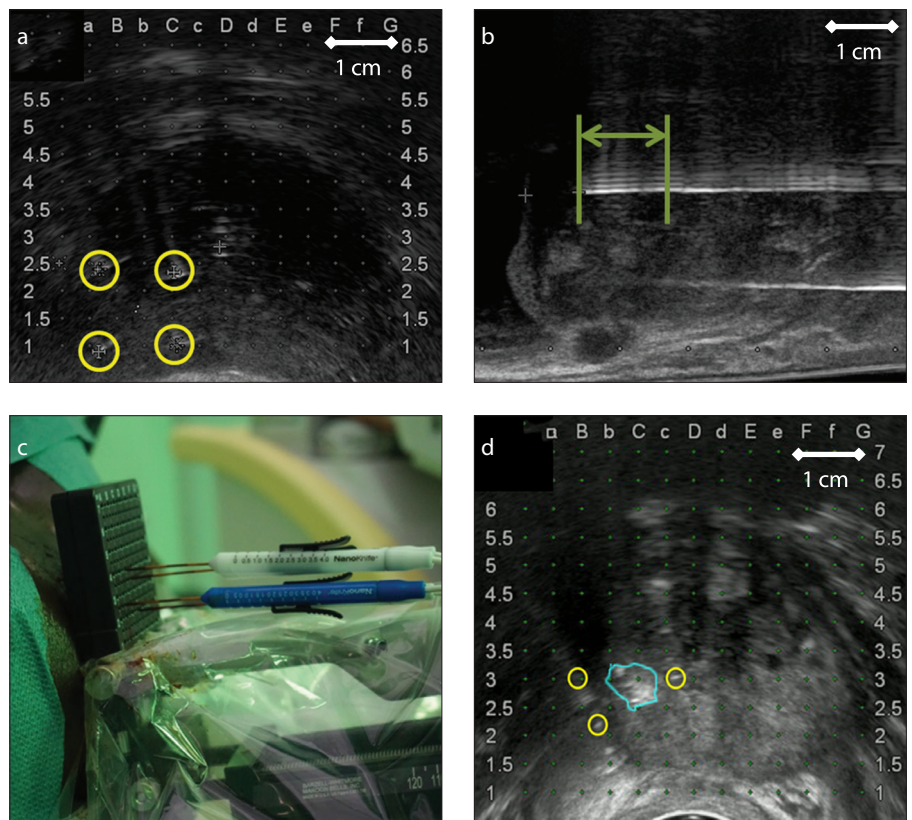

Figure 2. a–d. Needle electrode placement *(yellow circles)* with transrectal ultrasound (TRUS)-guidance in sagittal **(a)** and longitudinal **(b)** view, the active tip length is marked between bars. The brachygrid **(c)** used for electrode placement and horizontal fixation. Electrolysis of water **(d)** can be seen as a hyperechogenic region *(delineated in blue)* within the electrode configuration *(yellow circles)*.

Biplanar TRUS allows exact IRE needle placement using both transverse and longitudinal view with mpMRI-TRUS cognitive fusion (Fig. 2a, 2b) or TTMB-based targeting. The brachygrid is used for needle placement and to achieve parallel electrode orientation by horizontal fixation (Fig. 2c). Consecutive electrical pulses were delivered with IRE and these shocks are visible with TRUS (Video 1. See corresponding video/movie images at https://doi.org/10.5152/dir.2017.16608). By generating a high-voltage direct current between

each electrode pair, the potential difference required to split water molecules is reached (electrolysis). Electrolysis of water can be seen on TRUS as hyperechogenic regions within the electrical field (Fig. 2d). The concurrent oxidation of chloride is believed to contribute to the ablative effect with IRE (21).

The ablation zone 4 weeks following IRE is shown on T2-weighted imaging in Fig. 3a, characterized by an absence of contrast enhancement on T1-weighted dynamic sequence with a symmetric wall of reactive enhancement surrounding the ablation zone (Fig. 3b). Edema may be seen on T2-weighted imaging as areas with moderately increased T2-signal (Fig. 3a). At 6 months and 1 year, prostate deformations are observed, with low T2-signaling representing fibrosis (Fig. 3c, 3d).

CEUS visualized the ablation zone at 4 weeks following IRE as sharply demarcated nonperfused tissue compared with perfused tissue outside the ablation zone (Fig. 4a). At 6 months and 1 year, deformation of the ablation zone within the prostate was observed; however, treated areas could still be visualized as nonperfused areas (Fig. 4b, 4c).

Of the 16 patients that had mpMRI data available 4 weeks following IRE, 3 patients were excluded from analysis. In 1 patient the planned ablation zone was not correctly calculated due to a system error. The other 2 patients received an incomplete IRE treatment, one using 2 needle electrodes only with insufficient current output, whereas in the other case the inter-electrode distances were too far apart. The AZVs on T2-weighted MRI 4 weeks following IRE (n=13) had a mean (± standard deviation) volume of 12.9±7.0 cm^3 and were 5.3 times larger than the planned AZV (2.4±1.7 cm^3). The volumes on T2-weighted imaging and planning were positively correlated (P = 0.002) with a Pearson correlation coefficient of r=0.76 (Fig. 5a). The mean AZV for CEUS 4 weeks following IRE (n=8) was 20.7±8.7 cm^3 and was 8.5 times larger than the planned AZV. When compared, the volumes on CEUS and the planning showed a good positive correlation with a Pearson correlation coefficient of r=0.93 (P = 0.001) (Fig. 5b). Due to the prostate deformations and fibrosis, the AZV on imaging at 4 weeks, 6 months and 1 year differ. To illustrate this, the AZV on T2-weighted MRI is 3D reconstructed in Fig. 6 at 4 weeks (9.75 cm^3), 6 months (6.73 cm^3) and 1 year (6.46 cm^3) following IRE (n=1). At 4 weeks following IRE the prostate volume on MRI (n=15) is comparable with baseline MRI (mean increase, 4.4%±14.1%); however, due to the involution of the ablation zone the prostate volume on MRI at 6 months following IRE (n=6) is reduced with a mean reduction of 27.5%±11.9% compared with baseline prostate volume on MRI.

Residual or recurrent disease may be seen as a low T2-signal (Fig. 7a), asymmetrical enhancement on dynamic contrast-enhanced MRI (Fig. 7b), area with restricted diffusion on apparent diffusion coefficient maps and high signaling on diffusion-weighted imaging (b value >1000). Regions with focal early enhancement on CEUS within or outside the ablation zone may be indicative for residual/recurrent PCa (Fig. 7c). The suspicious area on Fig. 7 was histologically confirmed to be PCa Gleason 3+4=7, 10%–50% (adjacent to the ablation zone).
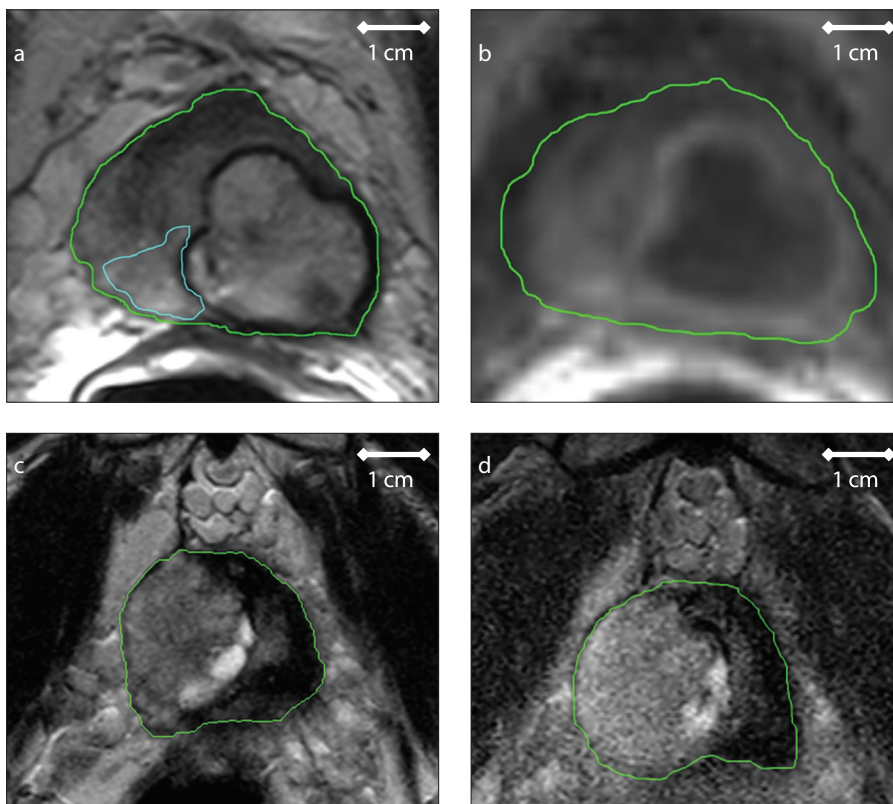

Figure 3. a–d. The ablation zone on follow-up. T2-weighted imaging **(a)** 4 weeks following IRE shows edema as moderately increased signal *(delineated in blue)*. T1-weighted dynamic imaging **(b)** shows absence of contrast enhancement within the ablation zone. T2-weighted images of the same ablation zone **(c, d)** show prostate deformations and a less clearly defined ablation zone at 6 months **(c)** and 12 months **(d)** following IRE.
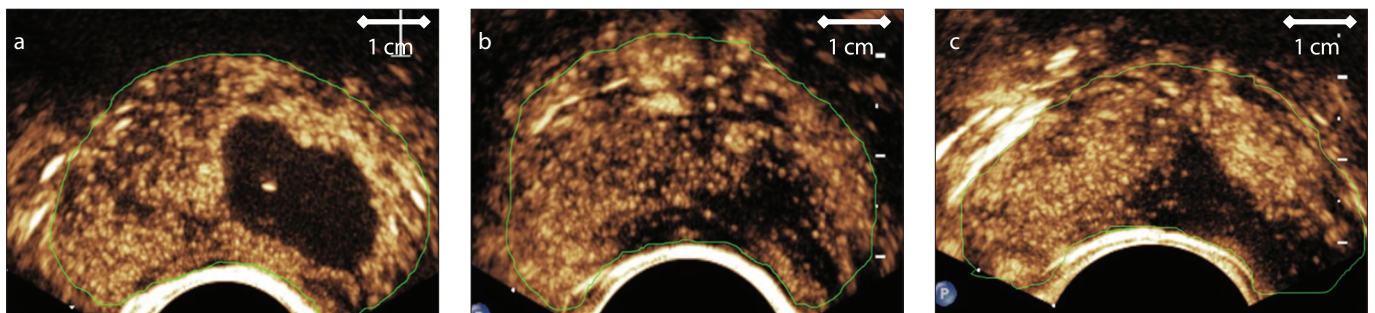

Figure 4. a–c. CEUS image 4 weeks following IRE **(a)** shows a sharply demarcated, nonperfused ablation zone. CEUS images at 6 months **(b)** and 12 months **(c)** following IRE show a less defined, nonperfused ablation zone with deformation.

a

$$y= 3{,}0809x + 5{,}3877$$
$$r= 0{,}76302$$

T2 MRI (cm³) vs **Planning (cm³)**

b

$$y= 4{,}6921x + 8{,}5528$$
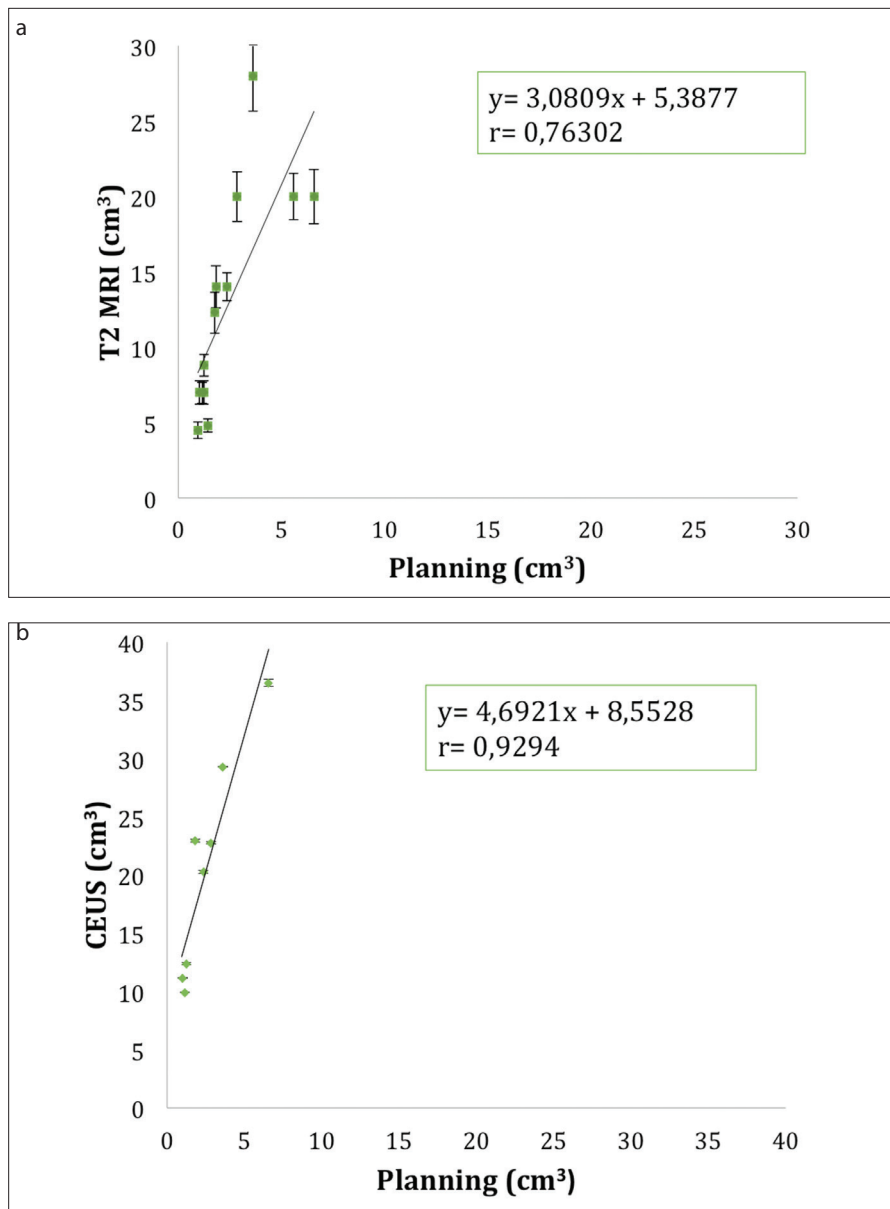$$r= 0{,}9294$$

CEUS (cm³) vs **Planning (cm³)**

Figure 5. a, b. Graph (**a**) shows the correlation between the ablation zone volume on T2-weighted imaging and treatment planning with a Pearson correlation coefficient of r=0.76. Graph (**b**) shows the correlation between the ablation zone volume on CEUS and treatment planning with a Pearson correlation coefficient of r=0.93.

Discussion

This report is the first to provide a descriptive overview on the use of mpMRI, CEUS, and TRUS for treatment planning, procedure guidance and follow-up following IRE for treatment of localized PCa. Unfortunately, no imaging modality is able to visualize the extent of the electrical field. Therefore, the extent of the ablation zone cannot be monitored in real-time. In a previous ablate and resect study it was shown that all tissue within the electrode configuration was ablated (5). Therefore, we considered the area within the electrode configuration as the planned AZV. We correlated the planned AZV with post-IRE AZVs on MRI and CEUS and found a strong positive correlation. However, the AZVs were larger than the treatment planning. This may be in line with findings after whole mount histopathologic analysis, which showed an extended ablation zone in relation to the electrode configuration, 2.5 to 2.9 times the surface area within the electrode configuration (5). CEUS may show a stronger correlation with the planned AZV than T2-weighted MRI since the 3 mm slice thickness with mpMRI inherently causes less accurate volume measurements. In order to improve treatment monitoring, and thereby reduce damage to vital adjacent structures, a correct mathematical model for the extent of ablation zone or a real-time monitoring imaging modality is required. Until such an option becomes available, postoperative imaging is the only possibility to provide feedback on the planned AZV. As the AZV seen on T2-weighted MRI and CEUS 4 weeks following IRE correlated well with AZV on whole mount pathology (r=0.88 and r=0.80, respectively) (9), this could also serve as feedback on treatment effectiveness.

In a consensus meeting on the follow-up of focal therapy it was stated that mpMRI should be performed at 6 months and then annually up to 5 years following focal therapy (10). Currently, no long-term follow-up data is available on IRE for localized PCa, in particular no data correlating imaging and treatment outcomes following IRE are available (4–8). There is a critical need for the quantitative validation of mpMRI following IRE, evaluating the ability to detect residual or recurrent PCa by use of standardized follow-up biopsies. Until this data becomes available, descriptive reports must provide clinicians with an overview on what imaging modalities can be used and what information from imaging results can be expected.

Imaging is an important aspect for every step in an IRE treatment protocol, from patient selection, treatment planning, and treatment guidance to follow-up. Currently, none of the existing imaging modality is able to visualize the electric field, nor the precise real-time formation of the ablation zone. CEUS and mpMRI may provide essential treatment-feedback by visualizing the ablation zone dimensions and volume 4 weeks following IRE. Long-term reproduced data on the utility of CEUS and mpMRI following IRE are required to construct optimal imaging-based follow-up protocols.

Video 1. Ultrasound imaging during the delivery of electrical pulses with IRE.
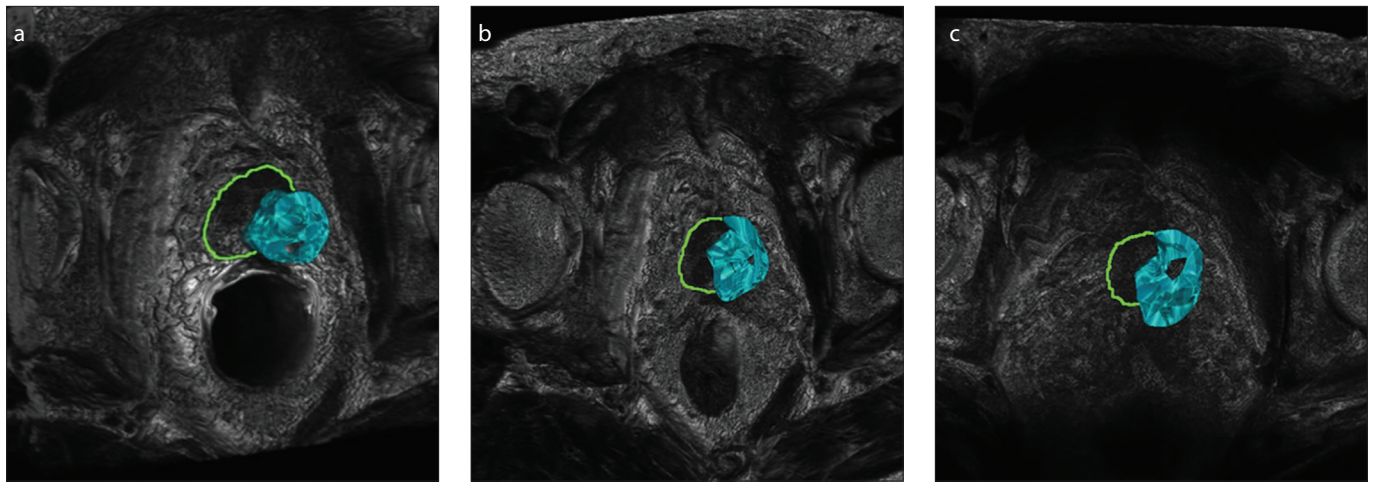https://doi.org/10.5152/dir.2017.16608

Figure 6. a–c. Three-dimensional reconstruction of the ablation zone at 4 weeks (**a**), 6 months (**b**) and 12 months (**c**) following IRE.
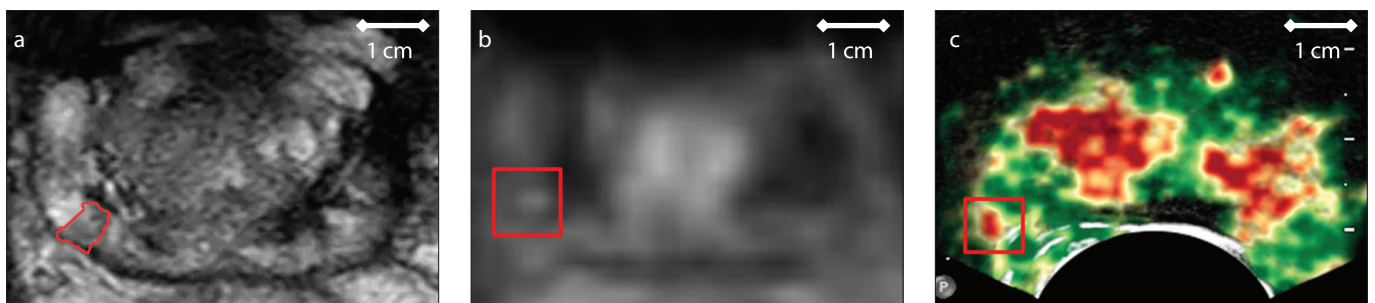

Figure 7. a–c. Six months following IRE, T2-weighted image (**a**) shows residual disease adjacent to the ablation zone *(delineated in red)*, DCE (**b**) shows asymmetrical enhancement, and CEUS contrast ultrasound dispersion imaging map (**c**) shows rapid focal enhancement.

References

1. Valerio M, Ahmed HU, Emberton M, et al. The role of focal therapy in the management of localised prostate cancer: a systematic review. Eur Urol 2013; 66:732–751. **[CrossRef]**

2. Davalos RV, Mir LM, Rubinsky B. Tissue ablation with irreversible electroporation. Ann Biomed Eng 2005; 33:223–231. **[CrossRef]**

3. Lee EW, Wong D, Prikhodko SV, et al. Electron microscopic demonstration and evaluation of irreversible electroporation-induced nanopores on hepatocyte membranes. J Vasc Interv Radiol 2012; 23:107–113. **[CrossRef]**

4. Neal RE, Millar JL, Kavnoudias H, et al. In vivo characterization and numerical simulation of prostate properties for non-thermal irreversible electroporation ablation. Prostate 2014; 74:458–468. **[CrossRef]**

5. van den Bos W, de Bruin DM, Jurhill RR, et al. The correlation between the electrode configuration and histopathology of irreversible electroporation ablations in prostate cancer patients. World J Urol 2016; 34:657–664. **[CrossRef]**

6. Ting F, Tran M, Böhm M, et al. Focal irreversible electroporation for prostate cancer: functional outcomes and short-term oncological control. Prostate Cancer Prostatic Dis 2016; 19:46–52. **[CrossRef]**

7. Murray KS, Ehdaie B, Musser J, et al. Pilot study to assess safety and clinical outcomes of irreversible electroporation for partial gland ablation in men with prostate cancer. J Urol 2016; 196:883–890. **[CrossRef]**

8. Valerio M, Stricker PD, Ahmed HU, et al. Initial assessment of safety and clinical feasibility of irreversible electroporation in the focal treatment of prostate cancer. Prostate Cancer Prostatic Dis 2014; 17:343–347. **[CrossRef]**

9. van den Bos W, de Bruin DM, van Randen A, et al. MRI and contrast-enhanced ultrasound imaging for evaluation of focal irreversible electroporation treatment: results from a phase I-II study in patients undergoing IRE followed by radical prostatectomy. Eur Radiol 2015; 26:2252–2260. **[CrossRef]**

10. Muller BG, van den Bos W, Brausi M, et al. Follow-up modalities in focal therapy for prostate cancer: results from a Delphi consensus project. World J Urol 2015; 33:1503–1509. **[CrossRef]**

11. Scheltema MJ, Tay KJ, Postema AW, et al. Utilization of multiparametric prostate magnetic resonance imaging in clinical practice and focal therapy: report from a Delphi consensus project. World J Urol 2017; 35:695–701. **[CrossRef]**

12. Valerio M, Shah TT, Shah P, et al. Magnetic resonance imaging-transrectal ultrasound fusion focal cryotherapy of the prostate: a prospective development study. Urol Oncol Semin Orig Investig 2017; 35:150.e1–150.e7. **[CrossRef]**

13. van den Bos W, de Bruin DM, Muller BG, et al. The safety and efficacy of irreversible electroporation for the ablation of prostate cancer: a multicentre prospective human in vivo pilot study protocol. BMJ Open 2014; 4:e006382. **[CrossRef]**

14. Scheltema MJ, van den Bos W, de Bruin DM, et al. Focal vs extended ablation in localized prostate cancer with irreversible electroporation; a multi-center randomized controlled trial. BMC Cancer 2016; 16:299. **[CrossRef]**

15. Barentsz JO, Weinreb JC, Verma S, et al. Synopsis of the PI-RADS v2 guidelines for multiparametric prostate magnetic resonance imaging and recommendations for use. Eur Urol 2016; 69:41–49. **[CrossRef]**

16. Kuenen MPJ, Saidov TA, Wijkstra H, Mischi M. Contrast-ultrasound dispersion imaging for prostate cancer localization by improved spatiotemporal similarity analysis. Ultrasound Med Biol 2013; 39:1631–1641. **[CrossRef]**

17. Dickinson L, Ahmed HU, Allen C, et al. Magnetic resonance imaging for the detection, localisation, and characterisation of prostate cancer: Recommendations from a European consensus meeting. Eur Urol 2011; 59:477–494. **[CrossRef]**

18. van den Bos W, Jurhill RR, de Bruin DM, et al. Histopathological outcomes after irreversible electroporation for prostate cancer: results of an ablate and resect study. J Urol 2016; 196:552–559. **[CrossRef]**

19. Van Den Bos W, Muller BG, Ahmed H, et al. Focal therapy in prostate cancer: International multidisciplinary consensus on trial design. Eur Urol 2014; 65:1078–1083. **[CrossRef]**

20. Tran M, Thompson J, Böhm M, et al. Combination of multiparametric MRI and transperineal template-guided mapping biopsy of the prostate to identify candidates for hemi-ablative focal therapy. BJU Int 2016; 117:48–54. **[CrossRef]**

21. Rubinsky L, Guenther E, Mikus P, Stehling M, Rubinsky B. Electrolytic effects during tissue ablation by electroporation. Technol Cancer Res Treat 2016; 15: NP95–103. **[CrossRef]**